ACS OMEGA

Open Access



http://pubs.acs.org/journal/acsodf

Article

# Molecular Dynamic Simulation Study on Replacement of Methane Hydrates with Carbon Dioxide Under Different Temperatures, Pressures, and Concentrations of Ethylene Glycol

Ping Guo,* Yi-Lun Song, Huang Liu, Wan-Bo Zhang, and Jian-Fei Zhao

Cite This: *ACS Omega* 2024, 9, 19031−19042

Read Online

ACCESS | Metrics & More | Article Recommendations

**ABSTRACT:** In order to alleviate the world energy resources crisis, the research and development of natural gas hydrates has a very important economic value and strategic significance. The $CH_4$−$CO_2$ replacement method can not only achieve geological storage of carbon dioxide but also more effectively mine natural gas hydrates. Based on molecular dynamics theory and the properties of natural gas hydrates, this paper delves into the replacement of methane hydrate with carbon dioxide under different temperatures, pressures, and concentrations of ethylene glycol (EG). We established a $CO_2$−Hydrate model and three $CO_2$/EG−Hydrate models with different concentrations of EG, and we simulated the radial distribution function (RDF), mean square displacement (MSD), and relative density distribution of each particle in the system in different conditions. The higher the temperature, the more unstable the methane hydrates are, and the methane hydrates are more prone to decomposition. Compared with 280 and 290 K, the temperature of 270 K is more favorable for carbon dioxide molecules to enter the hydrate layer and form carbon dioxide hydrates. The changes in pressure have little impact on the decomposition of methane hydrates, the rupture of water cages of methane hydrates, and the number of carbon dioxide molecules entering the hydrate layer under temperatures of 280 K and pressures of 1, 4, and 7 MPa. But overall, a pressure of 1 MPa is more conducive for carbon dioxide molecules to enter the hydrate layer and form carbon dioxide hydrates. Adding EG to $CO_2$ molecules can inhibit the decomposition of methane hydrates. However, the higher the concentration of EG, the faster the decomposition of methane hydrates. The degree of fracture of the water cages in methane hydrates is greater under pure $CO_2$ conditions. Adding EG to $CO_2$ molecules is more conducive for $CO_2$ molecules to enter the hydrate layer and form carbon dioxide hydrates. This review is of great significance to improve the mining efficiency and $CO_2$ storage efficiency of the replacement of natural gas hydrates with $CO_2$.

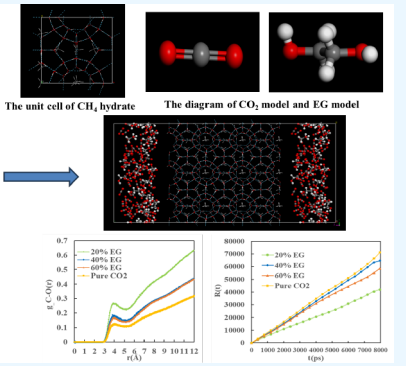


## 1. INTRODUCTION

The world today is facing a severe situation of reduced conventional oil and gas resources.[1] In order to alleviate the world energy resources crisis, the research and development of green energy−natural gas hydrates has very important economic value and strategic significance.[2] The products of the complete combustion of natural gas hydrates are carbon dioxide and water, making them an efficient and clean green energy source.[3] When the environmental temperature and pressure conditions of natural gas hydrates change, the phase equilibrium between molecules will be disrupted, causing the decomposition of natural gas hydrates.[4] Regarding this property of natural gas hydrates, scholars have proposed various natural gas hydrate mining technologies, mainly including the heat injection method, depressurization method, and chemical inhibitors injection method[5−12] But these traditional methods have certain drawbacks and are prone to environmental pollution.[13] With the in-depth research on the basic theory of natural gas hydrates in recent years, scholars have developed some new mining technologies, such as the $CH_4$−$CO_2$ replacement method, solid mining method[14−16] etc. The $CH_4$−$CO_2$ replacement method can not only achieve geological storage of carbon dioxide but also more effectively mine natural gas hydrates. Replacing methane hydrates with carbon dioxide has become a popular research direction for mining natural gas hydrate.[6]

In 1996, Ohgaki[17] conducted an experiment on the phase equilibrium of carbon dioxide replacing methane hydrates and found that methane hydrates can be converted into more stable carbon dioxide hydrates. Kim et al.[18] conducted experimental research and numerical simulation on the phase equilibrium relationships of $CO_2$ and $CH_4$ mixed gas hydrates in saline porous media systems. Wilder et al.[19] studied the

Received: December 2, 2023
Revised: January 23, 2024
Accepted: March 7, 2024
Published: April 16, 2024

formation process of mixed gas hydrates in porous medium. Smith et al.[20] studied the phase equilibrium conditions of $CH_4$ and $CO_2$ hydrates in porous glass with different pore sizes. Uchida et al.[21−23] studied the formation and decomposition process of mixed hydrates using Raman spectroscopy and gas chromatography. Seo et al.[24,25] studied the phase equilibrium characteristics of $CO_2$ and $CH_4$ mixed gas hydrates under isothermal conditions. Goel[26] conducted experimental research on the formation process of hydrates. Kvamme and Svandal et al.[27,28] found that $CO_2$ gas hydrates are more stable than $CH_4$ gas hydrates within a certain range of pressure and temperature. Sloan et al.[29] obtained the phase equilibrium diagram of the $CH_4$−$CO_2$−$H_2O$ system based on the phase equilibrium characteristics of $CH_4$ gas hydrates and $CO_2$ gas hydrates. Some scholars have studied the replacement efficiency of adding different types of chemical inhibitors to $CO_2$ gas hydrates[30−32]

Although traditional experimental methods have made significant progress, they cannot explain the mechanism of the replacement of $CH_4$ hydrate with $CO_2$ from a microscopic perspective. Molecular simulation has the characteristics of convenience and low cost. They can complete molecular performance research under harsh conditions and even some experimental studies that cannot be completed in practice, providing theoretical guidance for experimental research.

Geng et al.[33] studied the stability of $CH_4$ hydrates, $CO_2$ hydrates, and $CH_4$−$CO_2$ mixed gas hydrates under the conditions of $T$ = 260−280 K and $p$ = 5 MPa using molecular dynamics simulation methods. Yezdimer et al.[34] studied the feasibility of replacement of natural gas hydrate with $CO_2$ using molecular dynamics simulation methods. Hirohama et al.[35] believed that molecular fugacity is the driving force of the replacement process and proposed a related model. Qi et al.[36] simulated the stability of type I natural gas hydrates under the conditions of $T$ = 0−300 K using molecular dynamics methods. Geng et al.[33] simulated the stable structures of different types of mixed gas hydrates based on molecular dynamics theory. Tung et al.[37] simulated the effect of liquid $CO_2$ on the displacement of $CH_4$ hydrates. Lee et al.[38] found that $CO_2$ could replace $CH_4$ from natural gas hydrates, and there is a reverse reaction in this process. Some scholars have conducted simulation studies on the phase behavior of natural gas hydrates[39−41]

The previous research has problems, such as low efficiency of replacement of natural gas hydrates with $CO_2$. Therefore, based on molecular dynamics theory and the properties of natural gas hydrates, this paper delves into the replacement of methane hydrate with carbon dioxide under different temperatures, pressures, and concentrations of ethylene glycol (EG). We established a $CO_2$−Hydrate model and three $CO_2$/EG-Hydrate models with different concentrations of ethylene glycol, and we simulated the radial distribution function (RDF), mean square displacement (MSD), and relative density distribution of each particle in the system in different conditions. This article is of great significance in improving the mining efficiency and $CO_2$ storage efficiency of the replacement of natural gas hydrates with $CO_2$.

## 2. METHODS

To further explore the feasibility of replacing methane hydrates with carbon dioxide and clarify the effects of temperature, pressure, and concentration of ethylene glycol on the process of replacing methane hydrates with carbon dioxide, this section establishes a $CO_2$−Hydrate model. Based on molecular dynamics theory, we simulated the motion characteristics of carbon dioxide molecules, methane molecules in hydrate cages, and water molecules in hydrate cages under different ensembles, temperatures, and pressures. Then three $CO_2$/EG−Hydrate models with different concentrations of ethylene glycol were established and compared with the $CO_2$−Hydrate model to study the impact of different concentrations of ethylene glycol on the displacement of methane hydrates by carbon dioxide.

**2.1. Simulation Systems.** We established a $CO_2$−Hydrate model through the Build and Amorphous Cell modules of Materials Studio software. Among them, the typical unit cell of type I methane hydrate was established based on the atom spatial coordinates obtained from X-ray single crystal diffraction experiments in methane hydrate,[42] as shown in Figure 1. The methane hydrate part consists of a 3 × 3 x 3

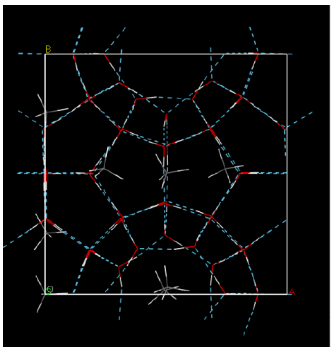

**Figure 1.** Unit cell of methane hydrate.

typical unit cell of type I methane hydrate, including 1242 water molecules and 216 methane molecules. The diagram of the $CO_2$ model and the ethylene glycol (EG) model is shown in Figure 2. We added the same $CO_2$ molecules on both sides

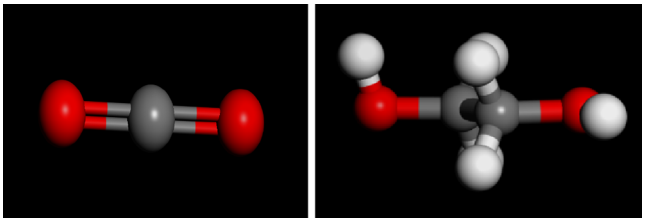

**Figure 2.** Diagram of the $CO_2$ model and the EG model.

of the hydrate cage simultaneously, totaling 200. The diagram of the $CO_2$−Hydrate model is shown in Figure 3, with box's side $a$ = $b$ = 34.86 Å and $c$ = 68.05 Å.

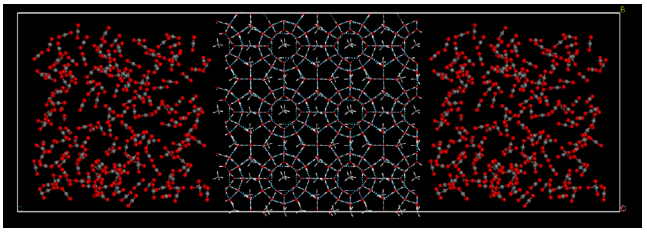

**Figure 3.** Diagram of the $CO_2$−Hydrate model.



https://doi.org/10.1021/acsomega.3c09630
ACS Omega 2024, 9, 19031−19042

The $CO_2$/EG−Hydrate models are divided into three types based on different concentrations of ethylene glycol(EG). The $CO_2$/EG−Hydrate model with the concentrations of EG of 20%, a total of 40 EG molecules, 160 $CO_2$ molecules, with box's side $a = b = 34.86$ Å, $c = 69.98$ Å, as shown in Figure 4;

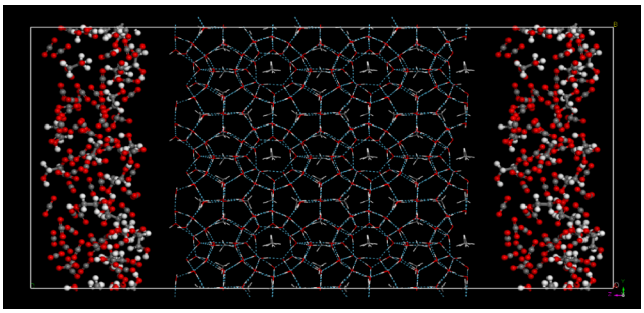

**Figure 4.** Diagram of the $CO_2$/EG−Hydrate model with a concentration of EG at 20%.

The $CO_2$/EG−Hydrate model with the concentrations of EG of 40%, a total of 80 EG molecules, 120 $CO_2$ molecules, with box's side $a = b = 34.86$ Å, $c = 73.05$ Å, as shown in Figure 5;

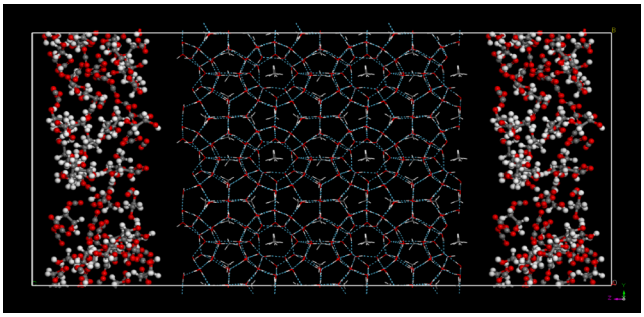

**Figure 5.** Diagram of the $CO_2$/EG−Hydrate model with a concentration of EG at 40%.

The $CO_2$/EG−Hydrate model with the concentrations of EG of 60%, a total of 120 EG molecules, 80 $CO_2$ molecules, with box's side $a = b = 34.86$ Å, $c = 74.39$ Å, as shown in Figure 6.

**2.2. Simulation Details.** When the model is established, the L−J (Lennard−Jones) potential energy model is used to calculate the interactions between $CH_4$ molecules and $H_2O$ molecules as well as between $CH_4$ molecules. The L-J potential energy parameters between molecules in hydrates are shown in Table 1.[43] The interactions between $H_2O$ molecules are

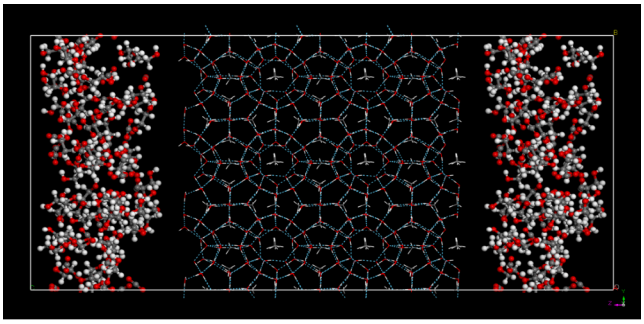

**Figure 6.** Diagram of the $CO_2$/EG−Hydrate model with a concentration of EG at 60%.

**Table 1. L−J Potential Energy Parameters Between Molecules in Hydrates**

| | $\varepsilon$/kJ mol$^{-1}$ | $\sigma$/Å |
|---|---|---|
| O−O | 0.65 | 3.16 |
| $CH_4$−O | 0.89 | 3.45 |
| $CH_4$−$CH_4$ | 1.23 | 3.73 |

described using the SPC (Simple Point Charge) potential energy model,[44] which includes van der Waals forces and electrostatic interactions:

$$u(r_{ij}) = \frac{q_i q_j}{4\pi\varepsilon_0 r_{ij}} + 4\varepsilon\left[\left(\frac{\sigma}{r_{ij}}\right)^{12} - \left(\frac{\sigma}{r_{ij}}\right)^{6}\right] \quad (1)$$

where $r_{ij}$ is the distance between water molecule $i$ and water molecule $j$; $u(r_{ij})$is the interaction between water molecule $i$ and water molecule $j$; $q_i$, $q_j$ is the number of charges of water molecule $i$ and water molecule $j$; $\varepsilon_0$ is the permittivity of vacuum; and $\varepsilon$, $\sigma$ are the parameters of the Lennard−Jones model.

During the simulation process, the boundaries in all three directions of the system are periodic boundary conditions, and the COMPASS force field is used to describe the molecular potential energy. Due to the edge length of a typical methane hydrate unit cell of approximately 11.62 Å, the simulated cutoff distance is taken as 12 Å. Take a time step of 1 fs and calculate the physical parameters related to the replacement reaction after the system is balanced. During the simulation process, output one frame every 5000 fs.

The $CO_2$/EG−Hydrate model was simulated using the canonical ensemble (NVT) and the constant-pressure, constant-temperature ensemble (NPT). At the beginning of the simulation, choose the Andersen constant temperature bath for temperature control and the Berendsen method for pressure control. To verify the feasibility of replacing methane hydrates with carbon dioxide, the replacement reaction process was simulated under the NVT ensemble at temperatures of 270, 280, and 290 K. So as to clarify the effects of temperature and pressure on the process of replacing methane hydrates with carbon dioxide, we simulated the replacement reaction process under the NPT ensemble at temperatures of 270 K, 280 K, 290 K and pressure conditions of 1, 4, and 7 MPa. To more intuitively study the effect of EG molecules with different concentrations on the displacement of methane hydrates by carbon dioxide, the Calculation module of MS software was used to simulate the kinetics characteristics of carbon dioxide molecules, methane molecules, and water molecules under the NPT ensemble at $p = 4$ MPa and $T = 280$ K. We also choose the Andersen constant temperature bath for temperature control and the Berendsen method for pressure control.

## 3. RESULT AND DISCUSSION

**3.1. Feasibility Verification of Replacing $CH_4$ Hydrates with $CO_2$.** To verify the feasibility of replacing methane hydrates with carbon dioxide, we simulated the replacement process of methane hydrate with carbon dioxide under the NVT ensemble at temperatures of 270, 280, and 290 K. The diagram of the system structure at different times at temperatures of 270, 280, and 290 K is shown in Figures 7−9.

From Figure 7, it can be seen that the methane hydrates in the system gradually decompose as the simulation progresses



https://doi.org/10.1021/acsomega.3c09630
ACS Omega 2024, 9, 19031−19042

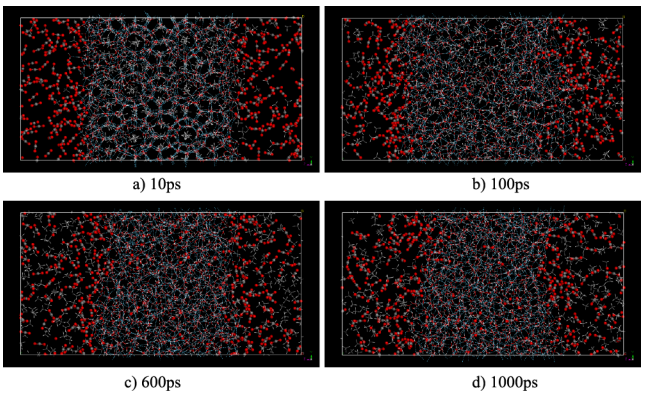


**Figure 7.** Diagram of the system structure at different times at a temperature of 270 K.

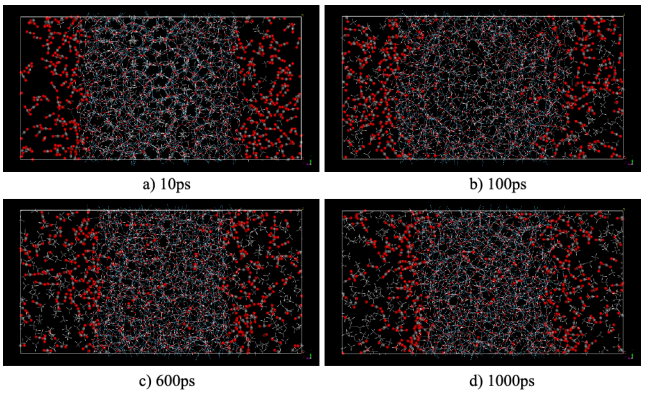


**Figure 8.** Diagram of the system structure at different times at a temperature of 280 K.

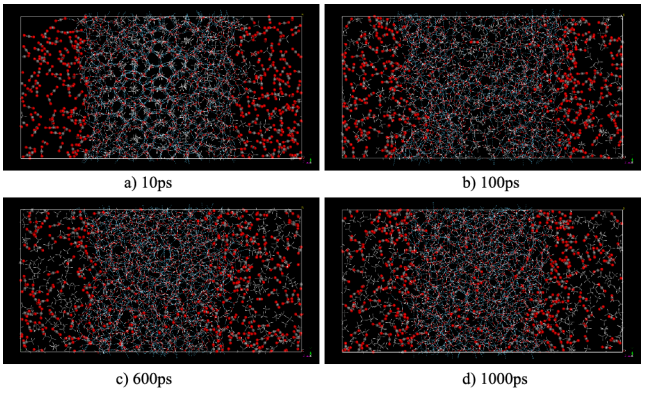


**Figure 9.** Diagram of the system structure at different times at a temperature of 290 K.

at a temperature of 270 K. At 10 ps, some methane hydrates at the junction of methane hydrates and $CO_2$ begin to decompose. At 100 ps, methane hydrates at the junction of methane hydrates and $CO_2$ have basically decomposed. At 600 ps, the methane hydrates inside the system begin to decompose, and $CO_2$ enters the methane hydrates layer. At 1000 ps, methane hydrates in the center of the hydrate layer have basically decomposed. Similarly, from Figures 8 and 9, it can be seen that methane hydrates in the system gradually decompose as the simulation progresses at temperatures of 280 and 290 K. Among them, at 600 ps, methane hydrates in the center of the hydrate layer have decomposed significantly.

In general, the water cage of methane hydrates gradually ruptures, and methane hydrates begin to decompose at temperatures of 270, 280, and 290 K. Methane molecules will diffuse out of the hydrate cage and initially gather together. In the early stages of the simulation, the fracture degree of the water cages of methane hydrates is relatively small. In the later stage of the simulation, a large number of water cages ruptured, but there are still some residual water cages. $CO_2$ molecules gradually enter the water cages of methane hydrates through the junction of methane hydrates and $CO_2$, and a small amount of $CO_2$ molecules enter the center of the hydrate layer. And the higher the temperature, the faster the decomposition of methane hydrates. The feasibility of replacing methane hydrate with carbon dioxide has been verified.

**3.2. The Influence of Temperature on the Replacement Process.** In order to study the effect of temperature conditions on the replacement of methane hydrates with carbon dioxide, we selected the constant-pressure, constant-temperature ensemble (NPT) to simulate the $CO_2$−Hydrate model. In addition, we analyzed the radial distribution function (RDF), mean square displacement (MSD) and relative density distribution of each particle in the system at temperatures of 270, 280, and 290 K under pressure of 3 MPa. And we compared the specific performance of replacing natural gas hydrates with carbon dioxide under different temperature conditions, as shown in Figures 10−12.

*3.2.1. The RDF Among the Atoms of the System at Different Temperatures.* From Figure 10a, it can be seen that the first characteristic peak of the radial distribution function (RDF) of $C(CH_4)$−$O(H_2O)$ at different temperatures is around $r$ = 4.21 Å, indicating the maximum regional density near this value. As the temperature increases, the value of the RDF gradually decreases. According to the definition of RDF, we know that the higher the temperature, the more unstable the methane hydrates are, and the methane hydrates are more prone to decomposition.

From Figure 10b, it can be seen that as the temperature increases, the RDF of the $O(H_2O)$−$O(H_2O)$ curve gradually decreases, and the second and third characteristic peaks gradually slow down. But the change in value is relatively small, indicating that the temperature has little effect on the degree of fracture of the water cage at temperatures of 270, 280, and 290 K. But the higher the temperature, the easier the water cages of methane hydrates are to rupture.

From Figure 10c, it can be seen that as the temperature increases, the RDF of $C(CO_2)$−$O(H_2O)$ gradually decreases, indicating that the optimal temperature for $CO_2$ to enter the water cage of methane hydrates and form carbon dioxide hydrates is 270 K. The difference between the RDF of $C(CO_2)$−$O(H_2O)$ at 290 and 280 K is small.

In general, the higher the temperature, the more unstable the methane hydrates are, and the methane hydrates are more prone to decomposition. The higher the temperature, the easier it is for the water cages of methane hydrates to rupture. The comparison of the displacement efficiency of the different studies[15] related to the influence of temperature shows that the higher the temperature, the more displacement is promoted and the higher the displacement efficiency can be acquired. The increase in temperature can also promote the penetration and diffusion rates of $CO_2$ molecules in the hydrate phase, and the formation rate of carbon dioxide hydrate is also accelerated. The consistency of the temperature can be verified by comparison with previous studies through experiments.


https://doi.org/10.1021/acsomega.3c09630
ACS Omega 2024, 9, 19031−19042

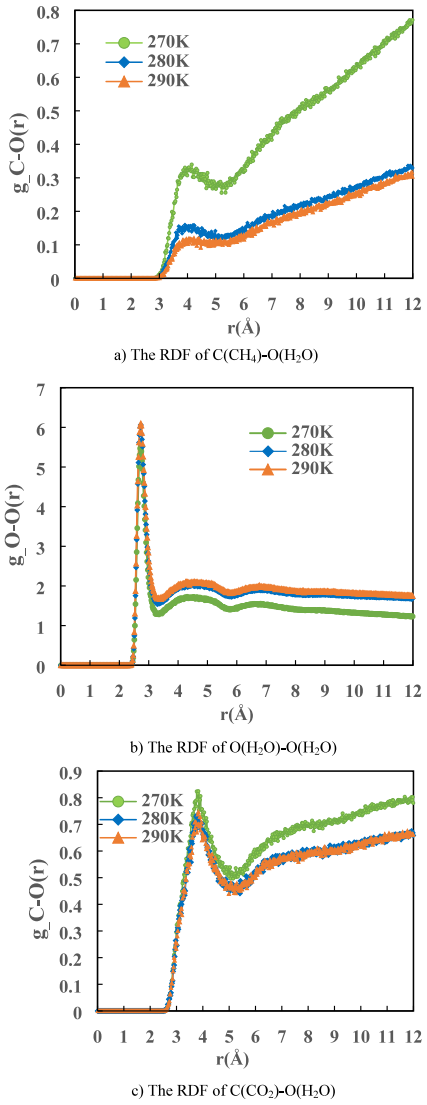


**Figure 10.** RDF among the atoms of the system at different temperatures.

*3.2.2. The MSD of Different Molecules at Different Temperatures.* The mean square displacement (MSD) represents the degree of deviation between the spatial position of molecules and their initial position in a system at a certain moment. Therefore, from Figure 11, it can be seen that as the temperature increases, the MSD of $CH_4$ molecules, $H_2O$ molecules, and $CO_2$ molecules gradually increases. As the simulation process progresses, the MSD curves at different temperatures show a straight upward trend. And the difference between 280 and 290 K is relatively small.

The MSD curves indicate that methane hydrates are not in a stable state and gradually decompose under pressure of 3 MPa and temperatures of 270, 280, and 290 K. As the temperature rises, the movement speed of methane molecules, carbon dioxide molecules, and water molecules increases. However, the increase in the MSD of water molecules is relatively small, which is consistent with the RDF of water molecules. The results indicate that the damage to the water cages of methane hydrates is relatively small, and there are still some residual water cages.

*3.2.3. The Relative Density Distribution at Different Temperatures.* The relative density distribution of different

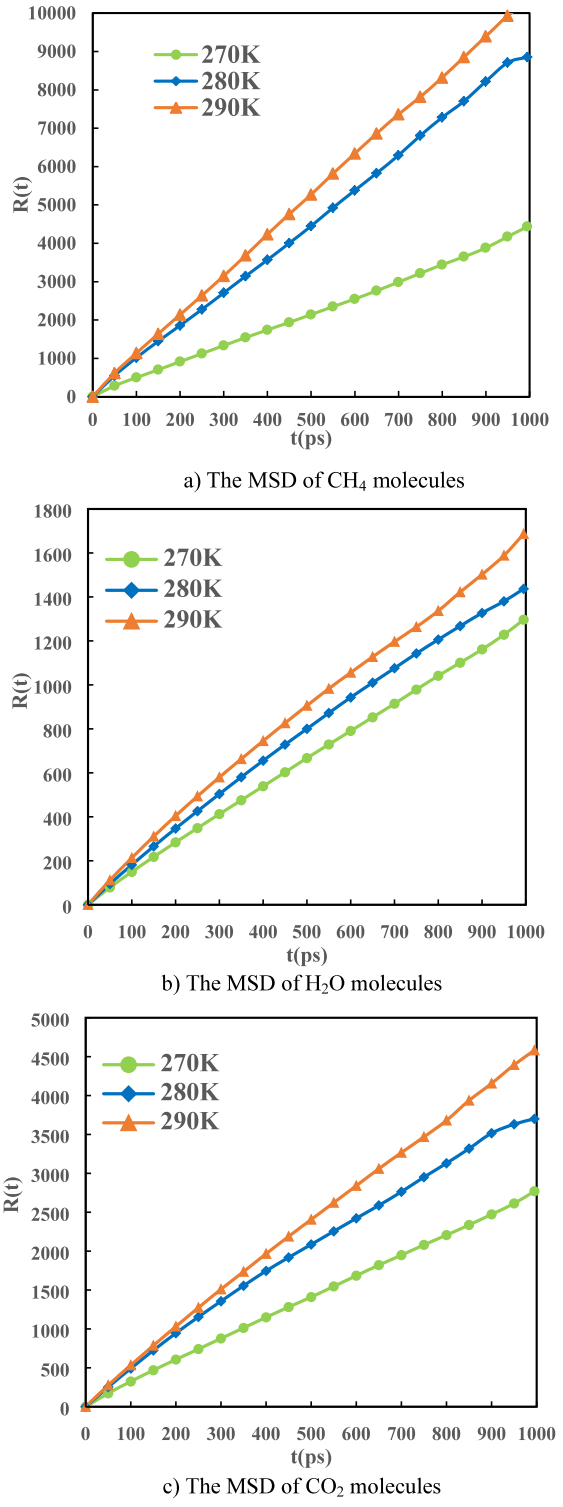


**Figure 11.** MSD of different molecules in the system at different temperatures.

molecules at different temperatures at $t$ = 2 ns is shown in Figure 12. For a more intuitive analysis of simulation results, the initial location of carbon dioxide is named zones I and III, and the initial location of the hydrate layer is named zone II. Figure 12 shows that there is still a large amount of methane hydrates that do not decompose at 270 K, while at 280 and 290 K, most methane hydrates decompose and $CH_4$ molecules



https://doi.org/10.1021/acsomega.3c09630
ACS Omega 2024, 9, 19031−19042

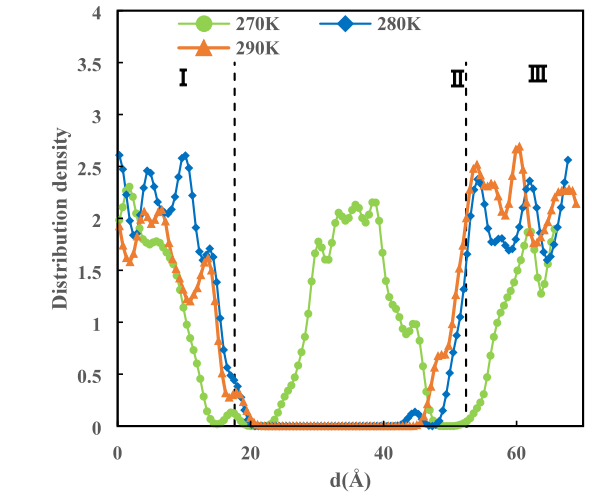


a) The relative density distribution of $CH_4$ molecules

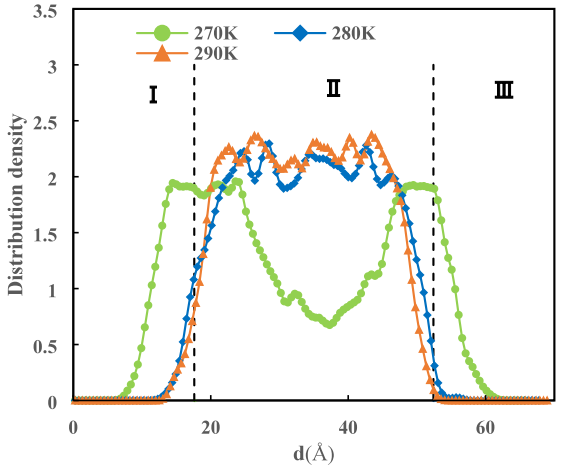


b) The relative density distribution of $H_2O$ molecules

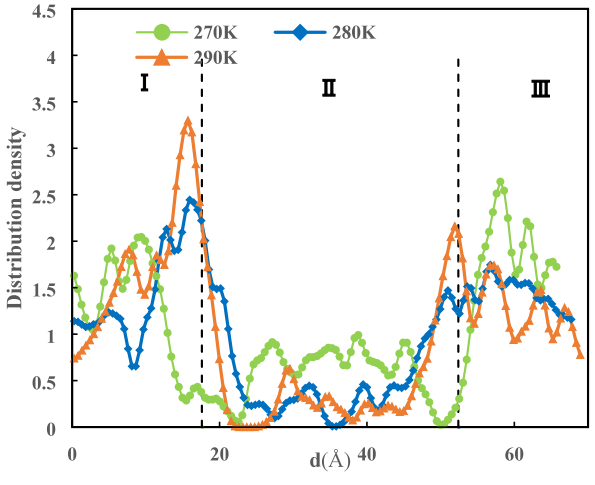


c) The relative density distribution of $CO_2$ molecules

**Figure 12.** Relative density distribution of different molecules at different temperatures.

diffuse into zones I and III. And the difference between 280 and 290 K is relatively small.

From Figure 12b, it can be seen that the relative density of $H_2O$ molecules in zone II under a temperature of 290 K is greater than the value under temperatures of 270 and 280 K, indicating that more water cages of methane hydrates are destroyed and water molecules gather in zone II under a temperature of 290 K. In addition, due to water is solid ice under a temperature of 270 K, the relative density is relatively small at 270 K. From Figure 12c, it can be seen that the number of carbon dioxide molecules in the zone II is higher at a temperature of 270 K, indicating that compared with 280 and 290 K, a temperature of 270 K is more favorable for carbon dioxide molecules to enter the hydrate layer and form carbon dioxide hydrates.

**3.3. The Influence of Pressure on the Replacement Process.** In order to study the effect of pressure conditions on the replacement of methane hydrates with carbon dioxide, we selected the constant-pressure, constant-temperature ensemble(NPT) to simulate the $CO_2$−Hydrate model. In addition, we analyzed the radial distribution function(RDF), mean square displacement(MSD) and relative density distribution of each particle in the system at pressures of 1, 4, and 7 MPa under temperature of 280 K. And we compared the specific performance of replacing natural gas hydrates with carbon dioxide under different pressure conditions, as shown in Figures 13−15.

*3.3.1. The RDF Among Atoms of the System at Different Pressures.* From Figure 13, it can be seen that the first characteristic peak of the radial distribution function (RDF) of $C(CH_4)$−$O(H_2O)$ at different pressures is around $r$ = 4.07 Å, indicating the maximum regional density near this value. As the pressure increases, the RDF of the $O(H_2O)$−$O(H_2O)$ curve gradually decreases, and the second and third characteristic peaks gradually slow down. The first characteristic peak of the radial distribution function (RDF) of $C(CO_2)$-$O(H_2O)$ at different pressures is around $r$ = 3.8 Å, followed by a trough and gradually rising, indicating that carbon dioxide molecules enter the hydrate layer mainly at the junction of methane hydrates and $CO_2$.

In general, as the pressure increases, the RDF of $C(CH_4)$−$O(H_2O)$, $O(H_2O)$−$O(H_2O)$, and $C(CO_2)$−$O(H_2O)$ of the system at different pressures has little change. The results indicate that the changes in pressure have little impact on the decomposition of methane hydrates, the rupture of water cages of methane hydrates, and the number of carbon dioxide molecules entering the hydrate layer under temperature of 280 K and pressures of 1, 4, and 7 MPa. But overall, a pressure of 1 MPa is more conducive for carbon dioxide molecules to enter the hydrate layer and form carbon dioxide hydrates.

*3.3.2. The MSD of Different Molecules at Different Pressures.* The mean square displacement (MSD) represents the degree of deviation between the spatial position of molecules and their initial position in a system at a certain moment. From Figure 14, it can be seen that as the simulation process progresses, the MSD curves at different pressures all show a straight upward trend.

From Figure 14a, it can be seen that as the pressure increases, the MSD of $CH_4$ molecules gradually decreases, indicating that the higher the pressure, the slower the decomposition rate of $CH_4$ hydrates, and the slower the movement speed of $CH_4$ molecules. From Figure 14b, it can be seen that with the increase of pressure, the change in MSD of water molecules is relatively small, indicating that the changes in pressure have little impact on the rupture of water cages of methane hydrates and the movement speed of water molecules. From Figure 14c, it can be seen that as the pressure increases, the MSD of $CO_2$ molecules gradually decreases, indicating that the higher the pressure, the slower


https://doi.org/10.1021/acsomega.3c09630
ACS Omega 2024, 9, 19031−19042

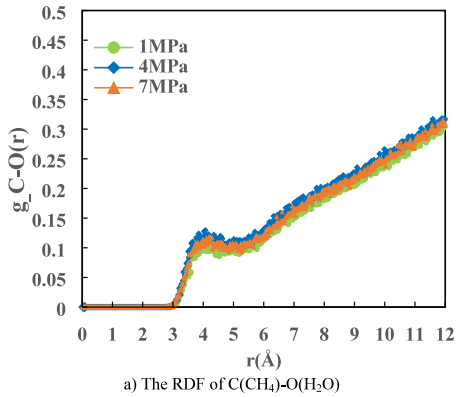


a) The RDF of $C(CH_4)$-$O(H_2O)$

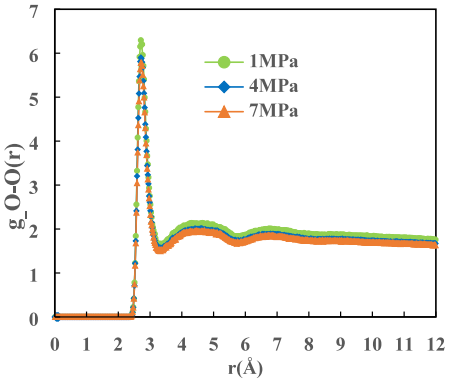


b) The RDF of $O(H_2O)$-$O(H_2O)$

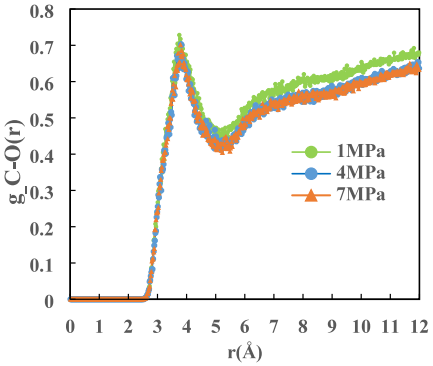


c) The RDF of $C(CO_2)$-$O(H_2O)$

**Figure 13.** RDF among the atoms of the system at different pressures.

the movement speed of $CO_2$ molecules. Some researchers believe that the lower the pressure is, the better it is for replacement. They found that the displacement efficiency actually decreases with the increase of $CO_2$ injection pressure, and the reduction of pressure can significantly improve the displacement rate of hydrate.[15] The lower the pressure, the greater the driving force of methane hydrate decomposition, which is more conducive to the decomposition of the $CH_4$ hydrate. The consistency of the pressure can be verified by comparison with previous studies through experiment.

*3.3.3. The Relative Density Distribution at Different Pressures.* The relative density distribution of different molecules at different pressures at $t$ = 2 ns is shown in Figure 15. For a more intuitive analysis of simulation results, the initial location of carbon dioxide is named as zones I and III, and the initial location of the hydrate layer is named as zone II.

From Figure 15a, it can be seen that the relative density of $CH_4$ molecules in zones I and III under pressure of 1 MPa is

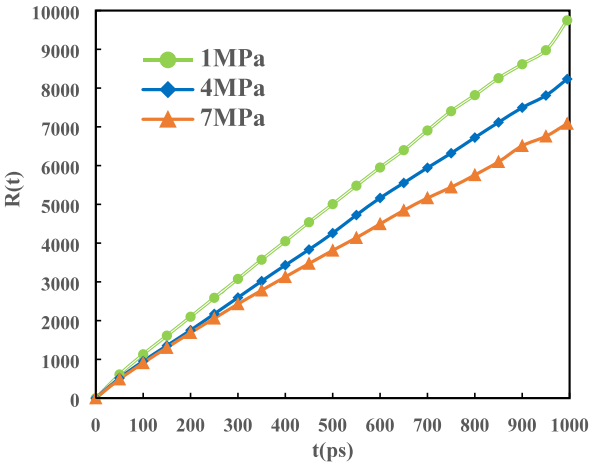


a) The MSD of $CH_4$ molecules

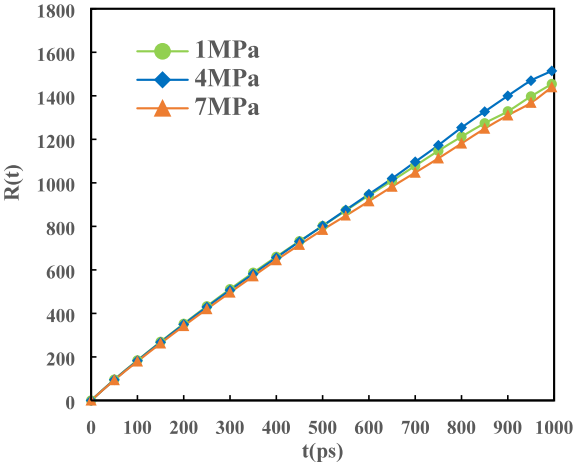


b) The MSD of $H_2O$ molecules

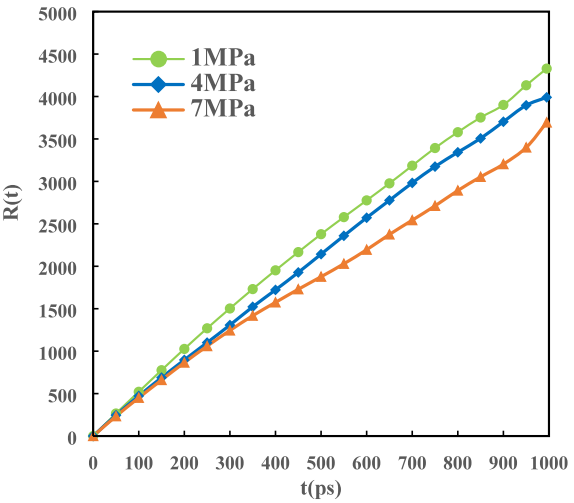


c) The MSD of $CO_2$ molecules

**Figure 14.** MSD of different molecules in the system at different pressures.

greater than the value under pressure of 4 and 7 MPa, indicating that under pressure of 1 MPa, more methane hydrates decompose and $CH_4$ molecules diffuse into zones I and III.

From Figure 15b, it can be seen that the relative density of $H_2O$ molecules in zone II under pressure of 1 MPa is greater than the value under pressures of 4 and 7 MPa, indicating that



https://doi.org/10.1021/acsomega.3c09630
ACS Omega 2024, 9, 19031−19042

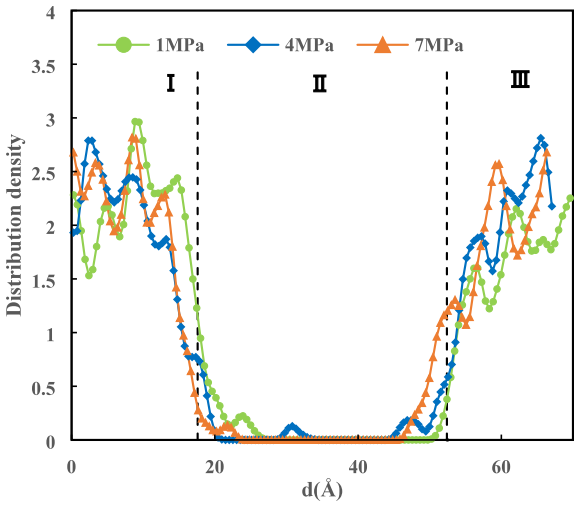


a) The relative density distribution of $CH_4$ molecules

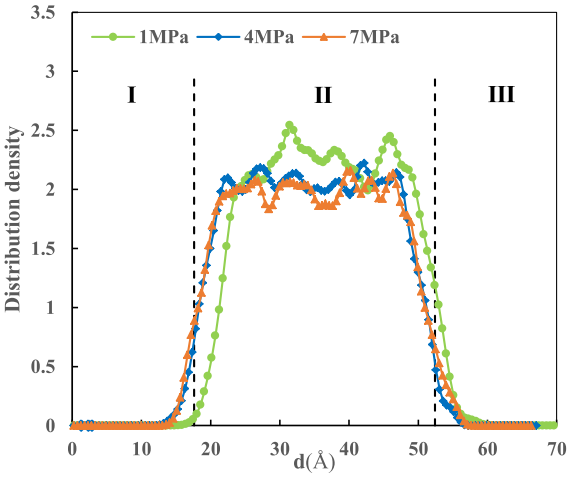


b) The relative density distribution of $H_2O$ molecules

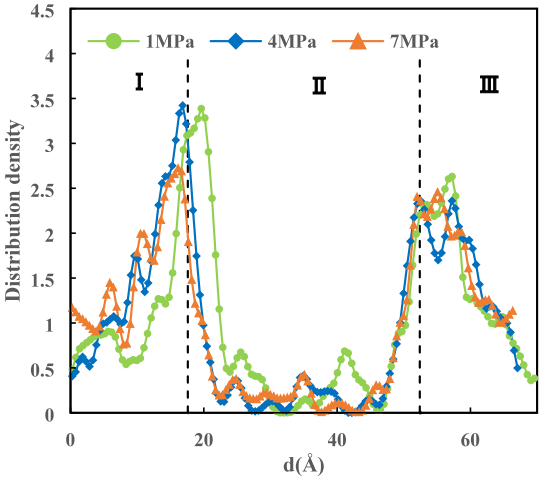


c) The relative density distribution of $CO_2$ molecules

**Figure 15.** Relative density distribution of different molecules at different pressures.

more water cages of methane hydrates are destroyed and water molecules gather in zone II under pressure of 1 MPa.

From Figure 15c, it can be seen that the relative density of $CO_2$ molecules in zone II is higher under pressure of 1 MPa, indicating that compared with pressures of 4 and 7 MPa, the pressure under 1 MPa is more favorable for carbon dioxide molecules to enter the hydrate layer and form carbon dioxide hydrates.

**3.4. The Effect of EG on the Replacement Process.** In order to study the effect of concentrations of ethylene glycol (EG) on the replacement of methane hydrates with carbon dioxide, we selected the constant-pressure, constant-temperature ensemble (NPT) to simulate the three $CO_2$/EG–Hydrate models. In addition, we analyzed the radial distribution function (RDF), mean square displacement (MSD), and relative density distribution of each particle in the system at a temperature of 280 K and a pressure of 4 MPa. And we compared the specific performance of replacing natural gas hydrates with carbon dioxide under different concentrations of EG, as shown in Figures 16–18.

*3.4.1. The RDF Among the Atoms at Different Concentrations of EG.* From Figure 16a, it can be seen that

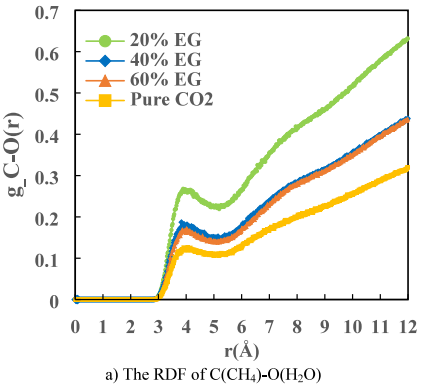


a) The RDF of $C(CH_4)$-$O(H_2O)$

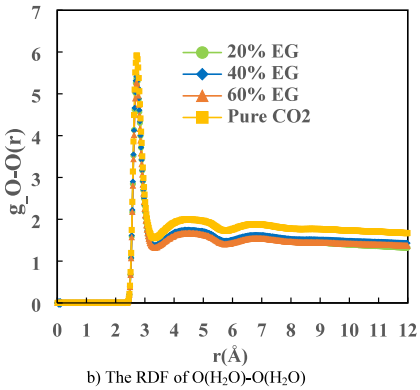


b) The RDF of $O(H_2O)$-$O(H_2O)$

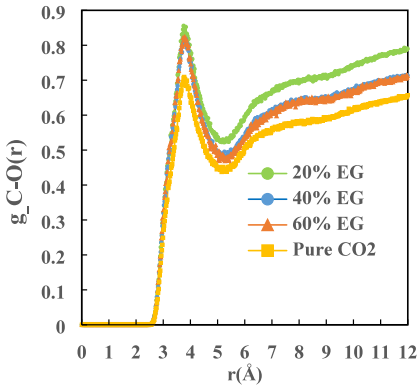


c) The RDF of $C(CO_2)$-$O(H_2O)$

**Figure 16.** RDF among the atoms of the system at different concentrations of EG.



https://doi.org/10.1021/acsomega.3c09630
ACS Omega 2024, 9, 19031–19042

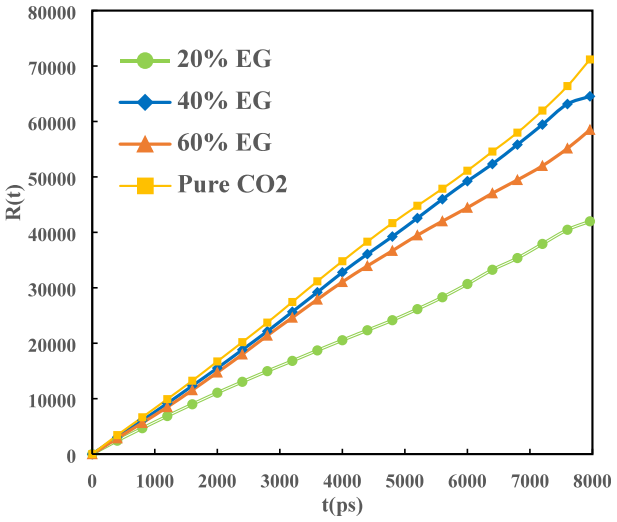


a) The MSD of $CH_4$ molecules

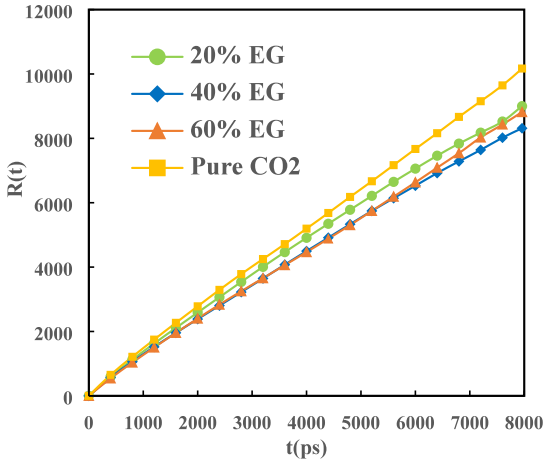


b) The MSD of $H_2O$ molecules

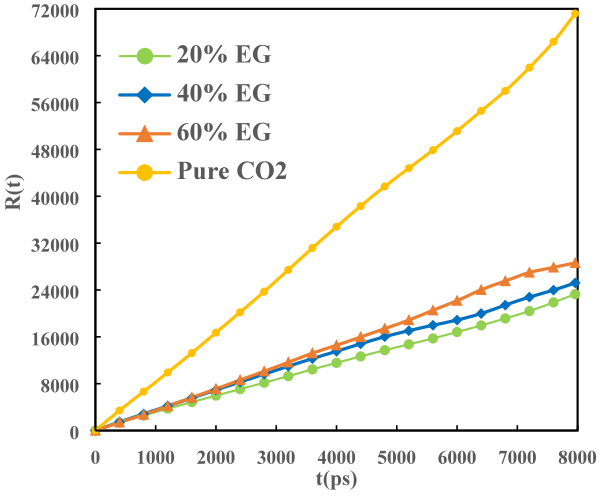


c) The MSD of $CO_2$ molecules

**Figure 17.** MSD of different molecules in the system at different concentrations of EG.

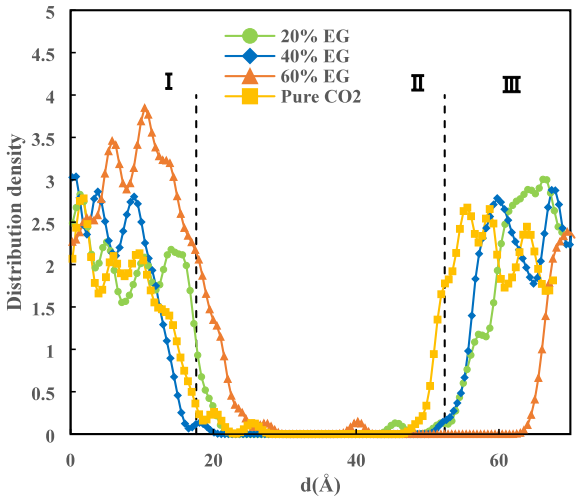


a) The relative density distribution of $CH_4$ molecules

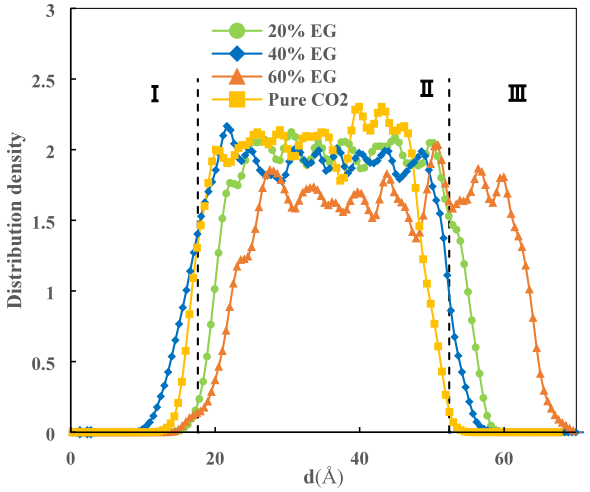


b) The relative density distribution of $H_2O$ molecules

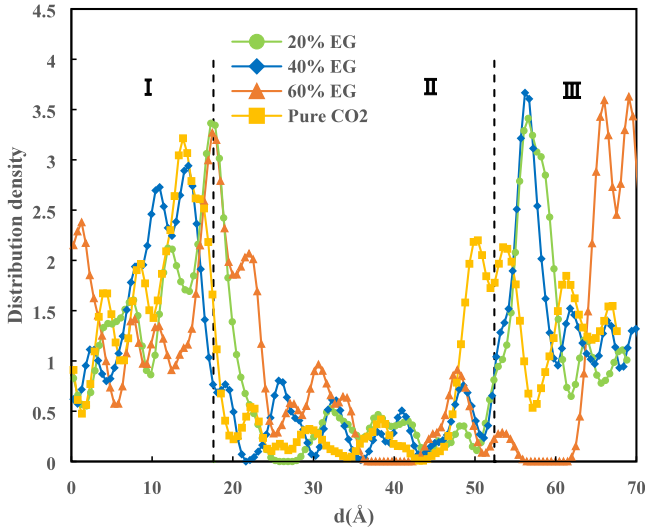


c) The relative density distribution of $CO_2$ molecules

**Figure 18.** Relative density distribution of different molecules at different concentrations of EG at 10 ns.

the first characteristic peak of the radial distribution function (RDF) of $C(CH_4)-O(H_2O)$ at different concentrations of EG is around $r$ = 3.9 Å, indicating the maximum regional density near this value. And the trend of the RDF curve is consistent.

As the concentration of EG increases, the value of the RDF of $C(CH_4)-O(H_2O)$gradually decreases, but all of them are larger than the value under pure $CO_2$ conditions, indicating



https://doi.org/10.1021/acsomega.3c09630
ACS Omega 2024, 9, 19031−19042

that adding EG to $CO_2$ molecules can inhibit the decomposition of methane hydrates. However, the higher the concentration of EG, the faster the decomposition of methane hydrates, with no significant difference between the concentrations of EG at 40% and 60%.

From Figure 16b, it can be seen that the RDF of $O(H_2O)$−$O(H_2O)$ at different concentrations of EG is basically the same, but all of them are lower than the value under pure $CO_2$ conditions, indicating that the degree of fracture of the water cages in methane hydrates is greater under pure $CO_2$ conditions. The change in the concentrations of EG has little effect on the degree of fracture of the water cages in methane hydrates.

From Figure 16c, it can be seen that as the concentration of EG increases, the value of the RDF of $C(CO_2)$-$O(H_2O)$ gradually decreases, but all of them are larger than the value under pure $CO_2$ conditions, indicating that adding EG to $CO_2$ molecules is more conducive for $CO_2$ molecules to enter the hydrate layer and form carbon dioxide hydrates. However, the higher the concentration of EG, the more difficult it is for $CO_2$ molecules to enter the water cages of methane hydrates, with no significant difference between the concentrations of EG at 40% and 60%.

*3.4.2. The MSD at Different Concentrations of EG.* The mean square displacement (MSD) represents the degree of deviation between the spatial position of molecules and their initial position in a system at a certain moment. From Figure 17, it can be seen that as the simulation process progresses, the MSD curves at different concentrations of EG all show a straight upward trend.

From Figure 17a, it can be seen that the MSD of $CH_4$ molecules under concentrations of EG at 40% and 60% is much greater than the value under concentrations of EG at 20%. And all of them are smaller than the value under pure $CO_2$ conditions. The results show that the decomposition rate of methane hydrates and the movement speed of methane molecules are faster under pure $CO_2$ conditions.

From Figure 17b, it can be seen that with the increase of the concentration of EG, the change in MSD of water molecules is relatively small, indicating that the changes in concentration of EG have little impact on the rupture of water cages of methane hydrates and the movement speed of water molecules.

From Figure 17c, it can be seen that as the concentration of EG increases, the MSD of $CO_2$ molecules gradually increases, and all of them are far smaller than the value under pure $CO_2$ conditions, indicating that the higher the concentration of EG, the faster the movement speed of the $CO_2$ molecules, but still far slower than the movement speed of the $CO_2$ under pure $CO_2$ conditions.

*3.4.3. The Relative Density Distribution of Different Molecules at Different Concentrations of EG.* The relative density distribution of different molecules at different concentrations of EG at $t$ = 10 ns is shown in Figure 18. For a more intuitive analysis of simulation results, the initial location of $CO_2$ and EG is named zones I and III, and the initial location of the hydrate layer is named zone II.

From Figure 18a, it can be seen that as the concentration of EG increases, the relative density of $CH_4$ molecules in zones I and III increases, and all of them are smaller than the value under pure $CO_2$ conditions, indicating that adding EG to $CO_2$ molecules can inhibit the decomposition of methane hydrates. From Figure 18b, it can be seen that as the concentration of EG decreases, the relative density of $H_2O$ molecules in zone II gradually increases, and all of them are smaller than the value under pure $CO_2$ conditions, indicating that as the concentration of EG decreases, more water cages of methane hydrates are destroyed and water molecules gather in zone II. From Figure 18c, it can be seen that the relative density of $CO_2$ molecules in zone II under pure $CO_2$ conditions is smaller than the value under different concentrations of EG, indicating that adding EG to $CO_2$ molecules can promote the formation of $CO_2$ molecules to enter the hydrate layer and form carbon dioxide hydrates.

## 4. CONCLUSION

Based on molecular dynamics theory, we established a $CO_2$−Hydrate model and three $CO_2$/EG−Hydrate models with different concentrations of EG, and we delved into the replacement of methane hydrate with carbon dioxide under different temperatures, pressures, and concentrations of ethylene glycol (EG). The main conclusions are as follows:

We compared the specific performance of replacing natural gas hydrates with carbon dioxide under different temperature conditions. The higher the temperature, the more unstable the methane hydrates are, and the methane hydrates are more prone to decomposition. Compared with 280 and 290 K, the temperature of 270 K is more favorable for carbon dioxide molecules to enter the hydrate layer and form carbon dioxide hydrates.

We compared the specific performance of replacing natural gas hydrates with carbon dioxide under different pressure conditions. The changes in pressure have little impact on the decomposition of methane hydrates, the rupture of water cages of methane hydrates, and the number of carbon dioxide molecules entering the hydrate layer under temperature of 280 K and pressures of 1, 4, and 7 MPa. But overall, a pressure of 1 MPa is more conducive for carbon dioxide molecules to enter the hydrate layer and form carbon dioxide hydrates.

We compared the three $CO_2$/EG−Hydrate models with the $CO_2$−Hydrate model. Adding EG to $CO_2$ molecules can inhibit the decomposition of methane hydrates. However, the higher the concentration of EG, the faster the decomposition of methane hydrates. The degree of fracture of the water cages in methane hydrates is greater under pure $CO_2$ conditions. Adding EG to $CO_2$ molecules is more conducive for $CO_2$ molecules to enter the hydrate layer and form carbon dioxide hydrates.

## AUTHOR INFORMATION


### Corresponding Author

**Ping Guo** − *State Key Lab of Oil and Gas Reservoir Geology and Exploitation, Southwest Petroleum University, Chengdu, Sichuan 610500, PR China;* orcid.org/0000-0003-2944-3123; Email: guopingswpi@vip.sina.com

### Authors

**Yi-Lun Song** − *State Key Lab of Oil and Gas Reservoir Geology and Exploitation, Southwest Petroleum University, Chengdu, Sichuan 610500, PR China*

**Huang Liu** − *State Key Lab of Oil and Gas Reservoir Geology and Exploitation, Southwest Petroleum University, Chengdu, Sichuan 610500, PR China*




https://doi.org/10.1021/acsomega.3c09630
ACS Omega 2024, 9, 19031−19042

**Wan-Bo Zhang** − *State Key Lab of Oil and Gas Reservoir Geology and Exploitation, Southwest Petroleum University, Chengdu, Sichuan 610500, PR China*

**Jian-Fei Zhao** − *State Key Lab of Oil and Gas Reservoir Geology and Exploitation, Southwest Petroleum University, Chengdu, Sichuan 610500, PR China*

Complete contact information is available at: https://pubs.acs.org/10.1021/acsomega.3c09630

### Notes

The authors declare no competing financial interest.

## ■ ACKNOWLEDGMENTS

This work was supported by the Research and Innovation Fund for Graduate Students of Southwest Petroleum University (2020CXZD31).

## ■ REFERENCES

(1) Zhang, Y.; Cui, M.; Xin, G.; Li, D. Microscopic insights on the effects of flue gas components on $CH_4$−$CO_2$ replacement in natural gas hydrate. *Gas Sci. Eng.* **2023**, *112*, 204947.

(2) Wang, T.; Sun, L.; Fan, Z.; Wei, R.; Li, Q.; Yao, H.; Dong, H.; Zhang, L.; Yang, L.; Zhao, J. Promoting $CH_4$/$CO_2$ replacement from hydrate with warm brine injection for synergistic energy harvest and carbon sequestration. *Chem. Eng. J.* **2023**, *457*, 141129.

(3) Castellani, B. Potential Pathway for Reliable Long-Term $CO_2$ Storage as Clathrate Hydrates in Marine Environments. *Energies* **2023**, *16* (6), 2856.

(4) Kvamme, B.; Vasilev, A. Thermodynamic Feasibility of the Black Sea $CH_4$ Hydrate Replacement by $CO_2$ Hydrate. *Energies* **2023**, *16* (3), 1223.

(5) Ul Haq, I.; Qasim, A.; Lal, B.; Zaini, D. B.; Foo, K. S.; Mubashir, M.; Khoo, K. S.; Vo, D.-V. N.; Leroy, E.; Show, P. L. Ionic liquids for the inhibition of gas hydrates. A review. *Environ. Chem. Lett.* **2022**, *20*, 2165−2188.

(6) Veluswamy, H. P.; NUpadhye, N. Review of Gas Hydrate Research in India: Status and Future Directions. *Energy Fuels* **2022**, *36*, 2323−2350.

(7) Ul Haq, I.; Lal, B.; Zaini, D. B. Experimental and modelling study of ammonium based ionic liquids in the absence and presence of methanol for $CO_2$ hydrates. *J. Mol. Liq.* **2022**, *349*, 118214.

(8) Sujith, K. S. Effect of methanol as an amphiphile on water structuring around a hydrate forming gas molecule: Insights from molecular dynamics simulations. *J. Mol. Liq.* **2022**, *361*, 119628.

(9) Giovannetti, R.; Gambelli, A. M.; Castellani, B.; Rossi, A.; Minicucci, M.; Zannotti, M.; Li, Y.; Rossi, F. May sediments affect the inhibiting properties of NaCl on $CH_4$ and $CO_2$ hydrates formation? an experimental report. *J. Mol. Liq.* **2022**, *359*, 119300.

(10) Rasoolzadeh, A.; Bakhtyari, A.; Mehrabi, K.; Javanmardi, J.; Nasrifar, K.; Mohammadi, A. H. Determination of clathrate hydrates stability conditions and water activity in aqueous solutions containing natural amino acid and its blend with ionic liquid, alcohol, and salt using a thermodynamic approach. *Fuel* **2022**, *326*, 124960.

(11) Gajanayake, S.; Pathegama Gamage, R.; Wanniarachchige, P. The influence of confining stresses on formation kinetics of methane gas hydrates. *Fuel* **2022**, *316*, 123257.

(12) Li, X.; Fan, S.; Wang, Y.; Li, G.; Wang, S.; Lang, X.; Liu, F. Hydrate phase equilibrium of hydrogen-natural gas blends: Experimental study and thermodynamic modeling. *Fluid Phase Equilib.* **2022**, *556*, 113417.

(13) Liu, H.; Li, H.; Yao, D.; Guo, P.; Wen, L. The research on the natural gas hydrate dissociation kinetic from hydrate-sediments/seawater slurries. *Chem. Eng. J.* **2022**, *435*, 135127.

(14) Ndlovu, P.; Babaee, S.; Naidoo, P. Review on $CH_4$-$CO_2$ replacement for $CO_2$ sequestration and $CH_4$/$CO_2$ hydrate formation in porous media. *Fuel* **2022**, *320*, 123795.

(15) Wei, W.-N.; Li, B.; Gan, Q.; Li, Y.-L. Research progress of natural gas hydrate exploitation with $CO_2$ replacement: A review. *Fuel* **2022**, *312*, 122873.

(16) Qi, R.; Qin, W.; Bian, H.; Lu, C.; Yu, L.; Ma, C. Overview of Molecular Dynamics Simulation of Natural Gas Hydrate at Nanoscale. *Geofluids* **2021**, *2021*, 1−17.

(17) Ohgaki, K.; Takano, K.; Sangawa, H.; Matsubara, T.; Nakano, S. Methane exploitation by carbon dioxide from gas hydrates—Phase equilibria for $CO_2$-$CH_4$ mixed hydrate system. *J. Chem. Eng. Jpn.* **1996**, *29* (3), 478−483.

(18) Kim, D. Y.; Seo, Y.; Lee, J. W.; Lee, H.. Thermodynamics and spectroscopic analysis of pure and mixed gas hydrates formed in porous media. In *The 15th Symposium on Thermophysical Properties*; University of Colorado: Boulder, 2003.

(19) Wilder, J. W.; Seshadri, K.; Smith, D. H. Thermodynamics of the sequestration of carbon dioxide in methane hydrates in porous media. *ACS Fuel Chem. Div. Prepr.* **2002**, *47* (1), 17−19.

(20) Smith, D. H.; Seshadri, K.; Uchida, T.; Wilder, J. W. Thermodynamics of methane, propane, and carbon dioxide hydrates in porous glass. *AIChE J.* **2004**, *50* (7), 1589−1598.

(21) Uchida, T.; Ikeda, I. Y.; Takeya, S.; Kamata, Y.; Ohmura, R.; Nagao, J.; Zatsepina, O. Y.; Buffett, B. A. Kinetics and Stability of $CH_4$−$CO_2$ Mixed Gas Hydrates during Formation and Long-Term Storage. *ChemPhysChem* **2005**, *6* (4), 646−654.

(22) Hachikubo, A.. Phase equilibrium and comparison of formation speeds of $CH_4$ and $CO_2$ hydrate below the ice point. In *Proceedings of the Fifth International Conference on Gas Hydrates*; Tapir Academic Press: Norway, 2005.

(23) Anderson, R.; Llamedo, M.; Tohidi, B.; Burgass, R. W. Experimental Measurement of Methane and Carbon Dioxide Clathrate Hydrate Equilibria in *Mesoporous Silica*. *J. Phys. Chem. B* **2003**, *107* (15), 3507−3514.

(24) Nakano, S.; Yamamoto, K.; Ohgaki, K. Natural gas exploitation by carbon dioxide from gas hydrate fields—high-pressure phase equilibrium for an ethane hydrate system. *Proc. Inst. Mech. Eng., Part A* **1998**, *212* (3), 159−163.

(25) Seo, Y.-T.; Lee, H. Multiple-phase hydrate equilibria of the ternary carbon dioxide, methane, and water mixtures. *J. Phys. Chem. B* **2001**, *105* (41), 10084−10090.

(26) Goel, N. In situ methane hydrate dissociation with carbon dioxide sequestration: Current knowledge and issues. *J. Pet. Sci. Eng.* **2006**, *51* (3−4), 169−184.

(27) Kvamme, B.; Tanaka, H. Thermodynamic stability of hydrates for ethane, ethylene, and carbon dioxide. *J. Phys. Chem.* **1995**, *99* (18), 7114−7119.

(28) Svandal, A.; Kuznetsova, T.; Kvamme, B. Thermodynamic properties and phase transitions in the $H_2O$/$CO_2$/$CH_4$ system. *Fluid Phase Equilib.* **2006**, *246* (1−2), 177−184.

(29) Sloan, Jr., E. D.; Koh, C. A. Estimation Techniques for Phase Equilibria of Natural Gas Hydrates. In *Proceedings of 3rd International Conference on Natural Gas Hydrates*, 2008; Francis Group: New York; pp 320523.

(30) Pandey, J. S.; Solms, N. V. Hydrate stability and methane recovery from gas hydrate through $CH_4$-$CO_2$ replacement in different mass transfer scenarios. *Energies* **2019**, *12* (12), 2309.

(31) Adibi, N.; Mohammandi, M.; Ehsani, M. R.; Khanmohammadian, E. Experimental investigation of using combined $CH_4$/$CO_2$ replacement and thermal stimulation methods for methane production from gas hydrate in the presence of $SiO_2$ and ZnO nanoparticles. *J. Nat. Gas Sci. Eng.* **2020**, *84*, 103690.

(32) Heydari, A.; Peyvandi, K. Study of biosurfactant effects on methane recovery from gas hydrate by $CO_2$ replacement and depressurization. *Fuel* **2020**, *272*, 117681.

(33) Geng, C. Y.; Wen, H.; Zhou, H. Molecular Simulation of the Potential of Methane Reoccupation during the Replacement of Methane Hydrate by $CO_2$. *J. Phys. Chem. A* **2009**, *113* (18), 5463−5469.

(34) Yezdimer, E. M.; Cummings, P. T.; Chialvo, A. A. Determination of the Gibbs Free Energy of Gas Replacement in SI

Clathrate Hydrates by Molecular Simulation. *J. Phys. Chem. A* **2002**, *106* (34), 7982−7987.
(35) Hirohama, S.; Shimoyama, Y.; Wakabayashi, A.; Tatsuta, S.; Nishida, N. Conversion of $CH_4$-hydrate to $CO_2$-hydrate in Liquid $CO_2$. *J. Chem. Eng. Jpn.* **1996**, *29* (6), 1014−1020.
(36) Qi, Y. X.; Zhang, H. MD simulation of $CO_2$-$CH_4$ mixed hydrate on crystal structure and stability. *Adv. Mater. Res.* **2011**, *181*−*182* (2), 310−315.
(37) Tung, Y. T.; Chen, L. J.; Chen, Y. P.; Lin, S.-T. In situ methane recovery and carbon dioxide sequestration in methane hydrates: A molecular dynamics simulation study. *J. Phys. Chem. B* **2011**, *115* (51), 15295−15302.
(38) Kvamme, B.; Graue, A.; Buanes, T.; Kuznetsova, T.; Ersland, G. Storage of $CO_2$ in natural gas hydrate reservoirs and the effect of hydrate as an extra sealing in cold aquifers. *Int. J. Greenhouse Gas Control* **2007**, *1* (2), 236−246.
(39) Jensen, L.; Thomsen, K.; Von Solms, N.; Wierzchowski, S.; Walsh, M. R.; Koh, C. A.; Sloan, E. D.; Wu, D. T.; Sum, A. K. Calculation of Liquid Water−Hydrate−Methane Vapor Phase Equilibria from Molecular Simulations. *J. Phys. Chem. B* **2010**, *114* (17), 5775−5782.
(40) Conde, M. M.; Vega, C. Determining the three-phase coexistence line in methane hydrates using computer simulations. *J. Chem. Phys.* **2010**, *133* (6), 064507.
(41) Conde, M. M.; Vega, C.; McBride, C.; Noya, E. G.; Ramírez, R; Sesé, L. M. Can gas hydrate structures be described using classical simulations? *J. Chem. Phys.* **2010**, *132* (11), 114503.
(42) Kirchner, M. T.; Boese, R.; Billups, W. E.; Norman, L. R. Gas hydrate single-crystal structure analyses. *J. Am. Chem. Soc.* **2004**, *126* (30), 9407−9412.
(43) Berendsen, H. J. C.; Postma, J. P. M.; Gunsteren, W. F. V.; Hermans, J. Interaction Models for Water in Relation to Protein Hydration. *Jerusalem Symp. Quantum Chem. Biochem.* **1981**, *14* (2), 331−342.
(44) Jorgensen, W. L.; Madura, J. D.; Swenson, C. J. Optimized intermolecular potential functions for liquid hydrocarbons. *J. Am. Chem. Soc.* **1984**, *106* (22), 6638−6646.


https://doi.org/10.1021/acsomega.3c09630
*ACS Omega* 2024, 9, 19031−19042